PHYSICAL REVIEW B **85**, 140505(R) (2012)

Bose-Einstein condensation in liquid ^{4}He near the liquid-solid transition line

S. O. Diallo,[1] R. T. Azuah,[2,3] D. L. Abernathy,[1] R. Rota,[4] J. Boronat,[4] and H. R. Glyde[5]

[1]*Quantum Condensed Matter Division, Oak Ridge National Laboratory, Oak Ridge, Tennessee 37831, USA*
[2]*NIST Center for Neutron Research, Gaithersburg, Maryland 20742-2115, USA*
[3]*Department of Materials Science and Engineering, University of Maryland, College Park, Maryland 20742-2115, USA*
[4]*Departament de Física i Enginyeria Nuclear, Universitat Politeécnica de Catalunya, E-08034, Barcelona, Spain*
[5]*University of Delaware, Newark, Delaware 19716-2570, USA*

(Received 8 November 2011; revised manuscript received 13 February 2012; published 9 April 2012)

We present precision neutron scattering measurements of the Bose-Einstein condensate (BEC) fraction $n_0(T)$ and the atomic momentum distribution $n^\star(\mathbf{k})$ of liquid ^{4}He as a function of temperature at pressure $p = 24$ bars. Both the temperature dependence of $n_0(T)$ and of the width of $n^\star(\mathbf{k})$ are determined. The $n_0(T)$ can be represented by $n_0(T) = n_0(0)[1 - (T/T_\lambda)^\gamma]$ with a small $n_0(0) = 2.80 \pm 0.20\%$ and large $\gamma = 13 \pm 2$ for $T < T_\lambda$, indicating a strong interaction. The onset of BEC is accompanied by a significant narrowing of the $n^\star(\mathbf{k})$. The narrowing accounts for 65% of the drop in kinetic energy below T_λ and reveals an important coupling between BEC and $k > 0$ states. The experimental results are well reproduced by path integral Monte Carlo calculations.

DOI: 10.1103/PhysRevB.85.140505 PACS number(s): 67.80.bd, 03.75.Kk, 78.70.Nx

Bose-Einstein condensation (BEC) is pervasive in condensed matter and in the origin of spectacular properties.[1] BEC may be defined as the condensation of a macroscopic fraction of bosons into one single-particle state,[2,3] as the onset of long-range order in the one-body density matrix,[4] or in a pair function. The phase of the macroscopically occupied single-particle state or pair function introduces phase coherence in the system, which is the origin of superfluidity and superconductivity. Magnetic order is also regularly described[5] in terms of condensation. BEC in a gas of photons has been observed.[6] Particularly, remarkable properties in dilute gases in traps arise from BEC and superflow. In gases the fraction n_0 of bosons in the condensate can be 100%, and BEC is easier to observe than superflow. In contrast, in dense systems such as liquid ^{4}He, where n_0 is small, superflow was observed long before BEC.[7] To date, BEC is uniquely observed in helium in the dynamic structure factor using neutrons.[8–11]

Reports of possible superflow in solid helium[12–16] have stimulated renewed interest in BEC in dense Bose systems. Observation of BEC in solid helium would be an unambiguous verification of superflow but, as yet, and to the best of our knowledge, has not been observed.[17–19] To better understand BEC in dense systems we have measured[20] the condensate fraction in liquid ^{4}He at low temperature as a function of pressure up to solidification, $p = 25.3$ bars. The full atomic momentum distribution $n(\mathbf{k})$, and especially the impact of BEC on $n(\mathbf{k})$ in dense systems, is also of great interest.

In this Rapid Communication we report precision measurements of the temperature dependence of $n(\mathbf{k})$ and n_0 of liquid ^{4}He under pressure $p = 24$ bars. The measurements were made on the wide angular-range chopper spectrometer (ARCS) instrument at the Spallation Neutron Source (SNS), Oak Ridge National Laboratory (ORNL). Path integral Monte Carlo (PIMC) calculations are also reported. From the observed $n(\mathbf{k})$ we obtain a Bose-Einstein condensate fraction $n_0(T) = n_0(0)[1 - (T/T_\lambda)^\gamma]$ with $n_0(0) = 2.80 \pm 0.20\%$ and $\gamma = 13 \pm 2$ below the normal-superfluid transition temperature $T_\lambda = 1.86$ K. The small value of n_0 and the large value of γ signal a strong interaction in the liquid at 24 bars. In addition to BEC, the momentum distribution of the atoms above the condensate, denoted $n^\star(\mathbf{k})$, narrows below T_λ. With the improved statistical precision of data collected on ARCS, we are able to determine both the temperature dependence of $n_0(T)$ and the width of $n^\star(\mathbf{k})$ simultaneously. The temperature dependence of the width of $n^\star(\mathbf{k})$ below T_λ tracks $n_0(T)$. This signals a coupling between BEC and the occupation of the higher momentum states. Below T_λ, there is both BEC and a redistribution of occupation of the $k > 0$ states in an interacting Bose system.

At temperatures close to but above T_λ, the kinetic energy $\langle K\rangle$ is dominated by quantum zero-point motion and hence is relatively temperature independent. When the liquid is cooled below T_λ, the kinetic energy $\langle K\rangle$ drops precipitously, both due to the onset of BEC and as a result of a narrowing of $n^\star(\mathbf{k})$ with temperature. For example, at $p = 24$ bars and $T = 40$ mK the majority, approximately 65%, of the observed drop in $\langle K\rangle$ comes from the decrease in the width of $n^\star(\mathbf{k})$ while 35% arises from the onset of BEC. This means that determinations of the condensate fraction n_0 from the drop in $\langle K\rangle$ below T_λ must take account of this narrowing of $n^\star(\mathbf{k})$. Otherwise n_0 will be overestimated. The impact of the narrowing is relatively smaller at saturated vapor pressure (SVP) where n_0 is larger. However, this effect explains why determinations of n_0 from the $\langle K\rangle$ made assuming that all the drops in $\langle K\rangle$ below T_λ arise from BEC yield large values of n_0.[9,10,21] The temperature dependence of both $n_0(T)$ and the width of $n^\star(\mathbf{k})$ are well reproduced in PIMC calculations.

The atomic momentum distribution is observed in the dynamic structure factor $S(Q,\omega)$ at high momentum, $\hbar Q$, and energy, $\hbar\omega$, transfer. In this limit, denoted the impulse approximation (IA), the energy transfer to the sample by the scattered neutrons is quadratic in Q, and centered around the ^{4}He recoil line $E_r = \hbar^2 Q^2/2m$, as shown in Fig. 1. In the IA, $S(Q,\omega)$ is conveniently expressed in terms of the y-scaling variable $y = (\omega - \omega_r)/v_r$, yielding[8,9,11]

$$J_{\mathrm{IA}}(y) = v_r S(Q,\omega) = \int d\mathbf{k}\,\delta(y - k_Q)n(\mathbf{k}), \tag{1}$$

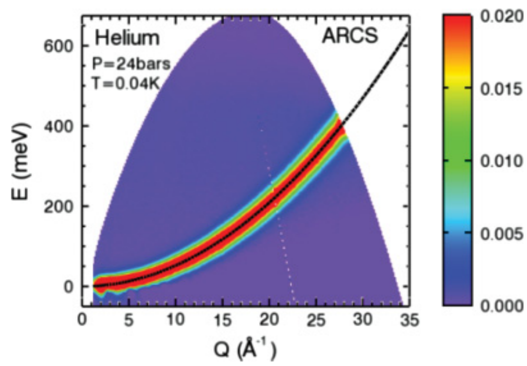

FIG. 1. (Color online) Observed scattering intensity $S(Q,\omega)$ as a function of energy transfer $E = \hbar\omega$ and momentum transfer $\hbar Q$ from liquid ^{4}He at $p = 24$ bars and $T = 40$ mK. The signal from the empty Al container has been subtracted. The black dashed line is the calculated ^{4}He recoil line $E_r = \hbar^2 Q^2/2m$, shown as a guide to the eye.

where $k_Q = k \cdot \frac{\mathbf{Q}}{|Q|}$ and $v_r = \hbar Q/m$. $J_{\rm IA}(y)$ is denoted the longitudinal momentum distribution and its Fourier transform $J_{\rm IA}(s)$, given by $J_{\rm IA}(s) = \int_{-\infty}^{+\infty} J_{\rm IA}(y)e^{-iys}dy$, is the one-body density matrix (OBDM) for displacements $s = \mathbf{r}\cdot\hat{\mathbf{Q}}$ along $\mathbf{Q}$. At finite Q, the observed $J(Q,y)$ is broadened by final-state interactions[22] and the instrument resolution. Accounting for these effects, single-particle dynamics, such as n_0, and $n(\mathbf{k})$ are directly observed from $J(Q,y)$.

The ARCS instrument was set in its high-resolution mode and a neutron incident energy $E_i = 700$ meV was selected to allow access to wave vectors up to $Q < 28$ Å^{-1}. Figure 1 displays the net two-dimensional (2D) contour map obtained from liquid ^{4}He after background subtraction. The measured instrument resolution function is compared in Fig. 2 with the ^{4}He $J(Q,y)$ response at $Q = 24$ Å^{-1} at temperatures below and above T_λ. The relative increase in intensity at $y = 0$ as the temperature is lowered below T_λ is attributed to the onset of BEC.

To analyze the data, we follow methods tested previously in liquid ^{4}He at SVP.[9,11,22–25] Specifically, we express $J(Q,s)$ as a product of the ideal $J_{\rm IA}(s)$ and the final-state (FS) function $R(Q,s)$.[22,25] $J_{\rm IA}(s)$ and $R(Q,s)$ are determined from fits to data. In order to extract a condensate n_0, we assumed as in previous work[22,25] a model momentum distribution $n(\mathbf{k})$ of the form

$$n(\mathbf{k}) = n_0[\delta(\mathbf{k}) + f(\mathbf{k})] + A_1 n^\star(\mathbf{k}), \tag{2}$$

where $n_0\delta(\mathbf{k})$ is the condensate component, $n^\star(\mathbf{k})$ is the distribution of atoms above the condensate in the $k \neq 0$ states, and $n_0 f(\mathbf{k})$ is a coupling between the two. The Fourier transform of $n^\star(\mathbf{k})$, $J^\star_{\rm IA}(s) = n^\star(s)$, expanded in powers of s up to s^6, is

$$n^\star(s) = \exp\left[-\frac{\bar{\alpha}_2 s^2}{2!} + \frac{\bar{\alpha}_4 s^4}{4!} - \frac{\bar{\alpha}_6 s^6}{6!}\right]. \tag{3}$$

The model $n(\mathbf{k})$ in Eq. (2) has thus four adjustable parameters, n_0, $\bar{\alpha}_2$, $\bar{\alpha}_4$, and $\bar{\alpha}_6$, that can be obtained by fits to experimental data. Including resolution effects, we were able to determine $n_0(T)$, the momentum distribution $n^\star(\mathbf{k})$, and the final-state function $R(Q,y)$.

To get a microscopic understanding of our data, we have carried out path integral Monte Carlo (PIMC) calculations of the momentum distribution liquid ^{4}He at the same densities and temperatures covered by the experiment.[26] PIMC is a microscopic stochastic method that is able to generate very accurate results relying only on the Hamiltonian of the system. The results here presented are obtained using a well-tested Aziz potential and a modern approach based on a high-order action and the worm algorithm for a better sampling of permutations.[27]

Figure 3 shows the parameters n_0 and $\bar{\alpha}_2$ obtained by fits to the experimental data at several Q values and at $T = 40$ mK. The variation with Q arises from the statistical uncertainty associated with the fitting procedure. The dashed lines indicate the corresponding average values. The fluctuation of the parameter values from Q to Q is small because the statistical precision of the data obtained on ARCS is high. The average condensate fraction $n_0$and the parameters $\overline{\alpha}_2$, $\overline{\alpha}_4$, and $\overline{\alpha}_6$

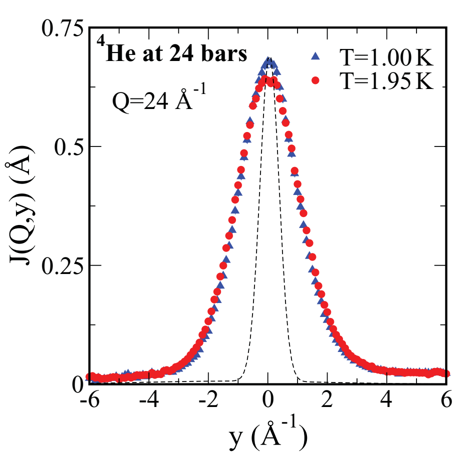

FIG. 2. (Color online) Observed $J(Q,y)$ at $Q = 24$ Å^{-1} and at the temperatures indicated. The black dashed line is the measured ARCS resolution function at $Q = 24$ Å^{-1}, which has a full width at half maximum (FWHM) of 0.76 Å^{-1}. The increased peak height at low temperature is attributed to the onset of BEC.

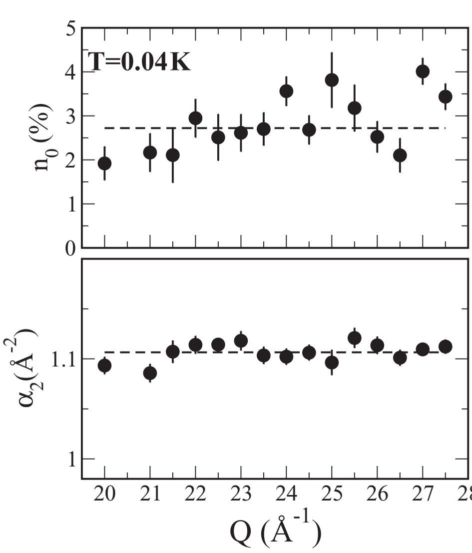

FIG. 3. The parameters $\bar{\alpha}_2$ and n_0 obtained by fits to data at several Q values and temperature $T = 40$ mK.

TABLE I. Temperature dependence of the condensate fraction n_0 and n(**k**) parameters in liquid ^{4}He under pressure $p = 24$ bars. The λ transition is at $T = 1.86$ K. The same parameters in liquid ^{4}He at SVP and in solid ^{4}He at $p = 41$ bars (Ref. [17]) are shown for comparison.

P (bar)	T (K)	n_0 (%)	$\bar{\alpha}_2$ (Å^{-2})	$\bar{\alpha}_4$ (Å^{-4})	$\bar{\alpha}_6$ (Å^{-6})
24	0.04	2.88 ± 0.60	1.10 ± 0.02	0.63 ± 0.10	1.35 ± 0.20
	1.00	2.96 ± 0.70	1.11 ± 0.02	0.62 ± 0.10	1.34 ± 0.15
	1.30	2.64 ± 0.75	1.11 ± 0.02	0.63 ± 0.10	1.28 ± 0.15
	1.50	2.56 ± 0.50	1.12 ± 0.01	0.61 ± 0.10	1.26 ± 0.25
	1.75	1.72 ± 0.70	1.15 ± 0.02	0.61 ± 0.10	1.27 ± 0.25
24	1.95	0.25 ± 1.65	1.19 ± 0.02	0.65 ± 0.20	0.95 ± 0.35
	3.50	0.32 ± 1.00	1.18 ± 0.02	0.56 ± 0.15	0.98 ± 0.30
	5.00	-0.04 ± 1.20	1.18 ± 0.02	0.53 ± 0.20	0.44 ± 0.60
SVP	0.50	7.25 ± 0.75	0.897 ± 0.02	0.46 ± 0.05	0.38 ± 0.04
41	0.12	0.08 ± 0.78	1.67 ± 0.05		

obtained by fits to data are listed in Table I. The dependence of $n_0(T)$ and $\overline{\alpha}_2(T)$ on temperature is shown in Figs. 4 and 5, respectively. From Table I and Fig. 4, we see that n_0 reaches a maximum value of $n_0 = 2.88 \pm 0.60\%$ at low temperature. The error bar on $n_0(0)$ is smaller because it is obtained as a fit to several observed n_0 values. As the temperature is decreased below $T_\lambda = 1.86$ K, $n_0(T)$ increases rapidly toward its maximum value. Essentially, $n_0(T)$ plateaus to its maximum value at temperatures close to $T_\lambda = 1.86$ K. This indicates that a strong interaction between the ^{4}He atoms limits n_0 at higher pressure with a decrease to the lowest temperatures unable to further reduce n_0. While the values of the parameters $\bar{\alpha}_4$ and $\bar{\alpha}_6$ in Table I are somewhat higher than those observed previously[20] at low temperature, the total low-temperature $n^\star(\mathbf{k})$ is the same and the value of n_0 at low T is independent of which $n^\star(\mathbf{k})$ is used.

In a Bose gas, $n_0(T) = n_0(0)[1 - (T/T_\lambda)^\gamma]$ with $n_0 = 100\%$ and $\gamma = 3/2$. A fit of this expression to the observed $n_0(T)$ in liquid ^{4}He at SVP gives $n_0(0) = 7.25 \pm 0.75\%$ and $\gamma = 5.5 \pm 1.0$.[25] A fit of the same expression to the present observed $n_0(T)$ at 24 bars gives $n_0(0) = 2.8 \pm 0.20\%$ and $\gamma = 13 \pm 2.0$. The fit is shown as a dashed line in Fig. 4. The large value of γ reflects the strong interaction in liquid ^{4}He at 24 bars.

From Table I and Fig. 5, we see that the parameter $\overline{\alpha}_2 = \langle |k_Q|^2 \rangle$, which sets the width of $n^\star(\mathbf{k})$, decreases from 1.18 Å^{-2} in the normal phase ($T > T_\lambda$) to 1.10–1.11 Å^{-2} at low temperature. That is, while $\overline{\alpha}_2$ is approximately independent of T in the normal phase, $\overline{\alpha}_2$ drops abruptly at temperatures immediately below T_λ. This abrupt decrease is unlikely to be a thermal effect since the thermal energy $k_B T_\lambda$ is already much less than the zero point energy (approximately $\langle K \rangle = 21.47$ K). Rather, the abrupt drop of $\overline{\alpha}_2$ below T_λ suggests a link to the onset of BEC. To test this picture we show the function $\overline{\alpha}_2(T) = \overline{\alpha}_2(T_\lambda) - \Delta[1 - (T/T_\lambda)^\gamma]$, where $\overline{\alpha}_2(T_\lambda) = 1.18$ Å^{-2}, $\Delta = \overline{\alpha}_2(T_\lambda) - \overline{\alpha}_2(0) = 0.08$ Å^{-2}, and $\gamma = 13$, which has the same temperature dependence as $n_0(T)$ as a dashed line in Fig. 5. The dashed line reproduces well the observed $\bar{\alpha}_2(T)$. Below T_λ, there appears to be a coupling between n_0 and $n^\star(\mathbf{k})$, perhaps of the same form of $n_0 f(\mathbf{k})$, which leads to a narrowing of $n^\star(\mathbf{k})$.

The narrowing of $n^\star(\mathbf{k})$ below T_λ is reproduced by PIMC calculations. The present PIMC values of $\overline{\alpha}_2$ are shown in Fig. 5 and they also decrease abruptly below T_λ. Thus the sharp reduction of $\overline{\alpha}_2$ below T_λ, to the best of our knowledge not observed previously, but observable with the

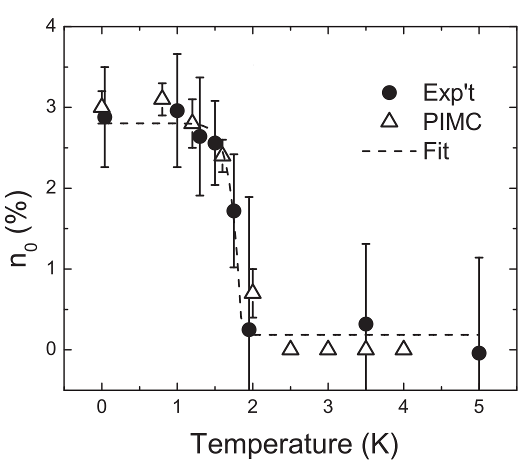

FIG. 4. Observed condensate fraction as a function of temperature. The dashed line is a line fit to the experimental data using $n_0(T) = n_0(0)[1 - (T/T_\lambda)^\gamma]$, where $T_\lambda = 1.86$ K. The open triangles are the simulated PIMC results.

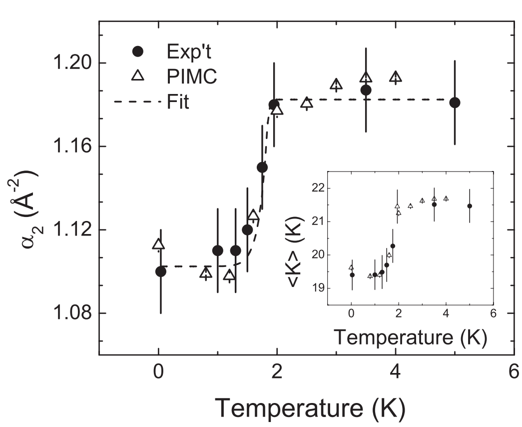

FIG. 5. Temperature dependence of the width $\bar{\alpha}_2$ of $n^\star(\mathbf{k})$ at $p = 24$ bars: simulation and experiment. The dashed line shows that $\bar{\alpha}_2(T)$ has a temperature dependence that tracks $n_0(T)$. The inset shows the corresponding $\langle K \rangle(T)$.

increased statistical precision of the data obtained on the ARCS instrument, is supported by accurate PIMC calculations. Below T_λ there is both BEC and a narrowing of $n^\star(\mathbf{k})$ in a strongly interacting Bose liquid.

In summary, the observed and PIMC values of $n_0(T)$ in liquid ^{4}He at 24 bars near the solidification line ($p = 25.3$ bars) are well represented by $n_0(T) = n_0(0)[1 - (T/T_\lambda)^\gamma]$, with $n_0(0) = 2.80 \pm 0.20\%$ and $\gamma = 13 \pm 2$. In a Bose gas $\gamma = 1.5$ and in liquid ^{4}He at SVP $\gamma = 5.5 \pm 1.0$. The large γ at 24 bars indicates a strong interaction in the liquid with n_0 saturating to a small value at temperatures close to T_λ. On cooling below T_λ, there is both BEC and a narrowing of the atomic momentum distribution of the atoms above the condensate $n^\star(\mathbf{k})$. The narrowing is characterized here by a drop in the width, $\bar{\alpha}_2 = \langle |k_Q|^2 \rangle$, of $n^\star(\mathbf{k})$. The temperature dependence of $\bar{\alpha}_2$ below T_λ tracks $n_0(T)$, indicating that the interaction between the condensate and the higher momentum states causes the narrowing of $n^\star(\mathbf{k})$. This coupling between n_0 and $n^\star(\mathbf{k})$ for $k > 0$ may be similar to the $n_0 f(\mathbf{k})$ term in Eq. (2) but changes $n(\mathbf{k})$ at higher k.

Both BEC and the narrowing of $n^\star(\mathbf{k})$ contribute to the drop in the $\langle K \rangle$ at temperatures below T_λ. The present observed and PIMC values of the temperature dependence of $n_0(T)$ and $\langle K \rangle$ at 24 bars agree well. At p = 24 bars, approximately 65% of the drop in $\langle K \rangle$ arises from the narrowing of $n^\star(\mathbf{k})$ below T_λ. Thus an n_0 obtained from the $\langle K \rangle$ assuming no narrowing of $n^\star(\mathbf{k})$ would significantly overestimate n_0. Indeed, if we apply the method to the present data at 24 bars, we get $n_0 = 7.5\%$ at 40 mK, which is more than two times the observed value. In the liquid at SVP where n_0 is larger, the relative reduction of the $\langle K \rangle$ arising from the narrowing of $n^\star(\mathbf{k})$ is smaller. However, it is still significant and in the future values of n_0 at SVP determined from the $\langle K \rangle$ must be corrected for this effect.

We thank J. Carmichael for designing the modular 100-bars sample cell and L. Solomon and E. Robles for valuable technical assistance with the sample environment. R.R. and J.B. acknowledge partial financial support from the DGI (Spain) Grant No. FIS2008-04403 and Generalitat de Catalunya Grant No. 2009SGR-1003. Work at ORNL and SNS is sponsored by the Scientific User Facilities Division, Office of Basic Energy Sciences, US DOE. This work was supported by the DOE, Office of Basic Energy Sciences under Contract No. ER46680.

[1] *Bose-Einstein Condensation*, edited by A. Griffin, D. Snoke, and S. Stringari (Cambridge University Press, Cambridge, UK, 1995).

[2] A. Einstein, Sitzungsber. Kgl. Preuss. Akad. Wiss. **1924**, 261 (1924).

[3] A. J. Leggett, Rev. Mod. Phys. **73**, 307 (2001).

[4] O. Penrose and L. Onsager, Phys. Rev. **104**, 576 (1956).

[5] T. Giamarchi, G. Ruegg, and O. Tchernyshyov, Nat. Phys. **4**, 198 (2008).

[6] J. Klaers, J. Schmitt, F. Vewinger, and M. Weitz, Nature (London) **468**, 545 (2010).

[7] P. Nozières and D. Pines, *Theory of Quantum Liquids Vol. II* (Addison-Wesley, Redwood City, CA, 1990).

[8] H. R. Glyde, *Excitations in Liquid and Solid Helium* (Oxford University Press, Oxford, UK, 1994).

[9] C. Andreani, D. Colognesi, J. Mayers, G. F. Reiter, and R. Senesi, Adv. Phys. **54**, 377 (2005).

[10] J. Mayers, C. Andreani, and D. Colognesi, J. Phys.: Condens. Matter **9**, 10639 (1997).

[11] R. N. Silver and P. E. Sokol, *Momentum Distributions* (Plenum, New York, 1989).

[12] E. Kim and M. H. W. Chan, Nature (London) **427**, 225 (2004).

[13] E. Kim and M. H. W. Chan, Science **305**, 1941 (2004).

[14] S. Balibar, Nature (London) **464**, 176 (2010).

[15] H. Choi, D. Takahashi, K. Kono, and E. Kim, Science **330**, 1512 (2010).

[16] E. J. Pratt, B. Hunt, V. Gadagkar, M. Yamashita, M. J. Graf, A. V. Balatsky, and J. C. Davis, Science **332**, 821 (2011).

[17] S. O. Diallo, J. V. Pearce, R. T. Azuah, O. Kirichek, J. W. Taylor, and H. R. Glyde, Phys. Rev. Lett. **98**, 205301 (2007).

[18] S. O. Diallo, R. T. Azuah, O. Kirichek, J. W. Taylor, and H. R. Glyde, Phys. Rev. B **80**, 060504 (2009).

[19] M. A. Adams, J. Mayers, O. Kirichek, and R. B. E. Down, Phys. Rev. Lett. **98**, 085301 (2007).

[20] H. R. Glyde, S. O. Diallo, R. T. Azuah, O. Kirichek, and J. W. Taylor, Phys. Rev. B **83**, 100507 (R) (2011).

[21] J. Mayers, F. Albergamo, and D. Timms, Physica B (Amsterdam) **276-278**, 811 (2000).

[22] H. R. Glyde, Phys. Rev. B **50**, 6726 (1994).

[23] V. F. Sears, Phys. Rev. B **30**, 44 (1984).

[24] G. Reiter and R. Silver, Phys. Rev. Lett. **54**, 1047 (1985).

[25] H. R. Glyde, R. T. Azuah, and W. G. Stirling, Phys. Rev. B **62**, 14337 (2000).

[26] J. Wilks, *The Properties of Liquid and Solid Helium* (Clarendon, Oxford, UK, 1967).

[27] R. Rota and J. Boronat, J. Low Temp. Phys. **162**, 146 (2011).